Journal of Biomechanics 102 (2020) 109659

Contents lists available at ScienceDirect

Journal of Biomechanics

journal homepage: www.elsevier.com/locate/jbiomech
www.JBiomech.com

Sensitivity of musculoskeletal model-based lumbar spinal loading estimates to type of kinematic input and passive stiffness properties

Ryan M. Byrne [a], Ameet K. Aiyangar [b,c,*], Xudong Zhang [d,e,f,*]

[a] Department of Mechanical Engineering, University of Pittsburgh, Pittsburgh, PA, USA
[b] Mechanical Systems Engineering, EMPA-Swiss Federal Laboratories for Materials Science and Technology, Duebendorf, Switzerland
[c] Department of Orthopaedic Surgery, University of Pittsburgh, Pittsburgh, PA, USA
[d] Department of Industrial & Systems Engineering, Texas A&M University, College Station, TX, USA
[e] Department of Biomedical Engineering, Texas A&M University, College Station, TX, USA
[f] Department of Mechanical Engineering, Texas A&M University, College Station, TX, USA

ARTICLE INFO

Article history:
Accepted 22 January 2020

Keywords:
Lumbar spinal loading
Subject-specific kinematics
Passive stiffness
Neutral position
Rigid-body musculoskeletal modeling

ABSTRACT

The study investigated the potential for obtaining more accurate spine joint reaction force (JRF) estimates from musculoskeletal models by incorporating dynamic stereo X-ray imaging (DSX)-based *in vivo* lumbar vertebral rotational and translational kinematics compared to generic, rhythm (RHY)-based kinematics, while also observing the influence of accompanying inputs: intervertebral segment stiffness and neutral state. A full-body OpenSim® musculoskeletal model, constructed by combining existing lower- and upper-body models, was driven based on one volunteer's (female; age 25; 60.8 kg; 176 cm) anthropometrics and kinematics from a series of upright standing and straight-legged dynamic lifting tasks. The lumbar spine portion was modified in a step-wise manner to observe effects of: (1) RHY vs. DSX lumbar kinematics; (2) No disc (bushing) stiffness (NBS); generic, linear bushing stiffness (LBS); subject-specific nonlinear bushing stiffness (NLBS); (3) Upright standing (UP) vs. Supine (SUP) neutral state; (4) Weight lifted: 4.5 kg vs. 13.6 kg. L4L5 JRF from 24 model variations based on combinations of aforementioned parameters were compared. Rhythm-based kinematics without translational components tends to over-predict JRF (31% and 39% for compression and shear, respectively) compared to DSX-based kinematics. Additionally, differences due to accompanying passive stiffness and neutral state choice combinations were even larger (>50%), indicating heightened demand on the quality of these accompanying inputs. The study not only highlights model sensitivity to choices made regarding the three primary inputs—kinematics, passive stiffness and neutral state— separately, but also how interactions between these choices can result in significant variability in joint loading estimates.

1. Introduction

Inverse dynamics-based multi-body musculoskeletal modeling is a commonly deployed approach for assessing mechanical loading within the lumbar spine. As with any modeling approach, the accuracy of resulting load predictions is sensitive to the quality of input parameters. Fundamental to modeling is the validity of simplifying assumptions governing two key sets of input parameters and their interaction: joint kinematics and passive tissue properties, particularly intervertebral disc (IVD) and ligament stiffnesses.

Under conventional assumptions, three rotational degrees of freedom (DOF) are sufficient for describing the kinematics of individual intervertebral joints (IVJ) comprising the lumbar spine; translational DOF are either non-existent, or, at best, small enough to only negligibly influence joint reaction force estimates (de Zee et al., 2007; Han et al., 2013; Pearcy and Bogduk, 1988). Second, individual IVJ rotations can be satisfactorily interpolated from the overall lumbar spinal rotations based on a fixed fractional distribution—lumbar spinal rhythm—throughout the entire range of a given movement (Arjmand and Shirazi-Adl, 2005; Bazrgari et al., 2008; Christophy et al., 2012; Tafazzol et al., 2014). Consequently, IVJ were routinely modelled in rigid body models as 3DOF spherical joints with their individual rotational contributions estimated based on a presumed lumbar rhythm. Over the last decade, however, new *in vivo* 6DOF intervertebral kinematic data acquired using technologies such as dynamic X-ray imaging have challenged

* Corresponding authors at: Mechanical Systems Engineering, EMPA-Swiss Federal Laboratories for Materials Science and Technology, Ueberlandstrasse 129, 8600, Duebendorf, Switzerland (A. Aiyangar).

E-mail addresses: ameet.aiyangar@empa.ch (A.K. Aiyangar), xudongzhang@tamu.edu (X. Zhang).

https://doi.org/10.1016/j.jbiomech.2020.109659
0021-9290/

these assumptions (Aiyangar et al., 2015; Aiyangar et al., 2014; Breen and Breen, 2018; Dehghan-Hamani et al., 2019; Eskandari et al., 2017; Xia et al., 2010; Zanjani-Pour et al., 2017).

The availability of *in vivo* subject-specific intervertebral kinematics presents a dilemma for modelers. On one hand, 6DOF kinematic datasets for individual IVJ based on direct vertebral motion measurements *theoretically* present the opportunity to obtain more accurate joint load estimates than was possible before. On the other hand, increased complexity of these datasets can not only lead to higher computational cost, but also impose a more stringent penalty for any errors within these datasets, heightening the demand on the accuracy of these parameters. For example, a recent *Monte Carlo* simulation-based study reported that even small translation component errors (0.1 – 0.3 mm) could induce large variations in IVJ force estimates (Eskandari et al., 2019).

IVD and ligament passive stiffness comprise the second key set of inputs. Solving a musculoskeletal inverse dynamics problem requires an accounting of the contribution of active (muscles) *and* passive (e.g. IVD and ligaments) components supporting the lumbar joint to properly satisfy the joint's measured generalized displacements, velocities, and accelerations during a specific movement. Passive reaction moments arising from IVD and ligament deformations contribute to the total reaction moment, thus altering the net moment contribution from the musculature and, consequently, the forces across muscles and resultant joint reaction forces (JRF). Hence, assumptions regarding representation of the IVD and ligaments could significantly affect simulation results. For instance, linear stiffness properties are often assumed (Gardner-Morse and Stokes, 2004; Meng et al., 2015; Senteler et al., 2018) for the inherently nonlinear IVD and ligaments (Panjabi et al., 1994), although recent studies have attempted to account for their nonlinearity (Ghezelbash et al., 2018). Further, the corresponding *in vivo* joint initial or "neutral position" and, consequently, the magnitudes of inherent pre-strain within these structures are not always known, thus creating an additional source of variability.

The current study investigated the potential for obtaining more accurate joint reaction and muscle force estimates by incorporating detailed and realistic, dynamic stereo X-ray imaging (DSX)-based 6DOF lumbar IVJ kinematics. It elucidates methodological aspects of incorporating these subject-specific lumbar kinematics into an OpenSim®-based (Delp et al., 2007; Seth et al., 2018; Seth et al., 2011; Sherman et al., 2013) full-body inverse dynamics-based musculoskeletal model, while observing the influence of accompanying input conditions (generic vs. subject-specific) and their interactions on L4L5 loading patterns and corresponding muscle forces during a set of sagittally symmetric dynamic lifting tasks. The following questions were investigated:

1) How do JRF estimates obtained with DSX-based subject-specific 6DOF IVJ kinematics differ from those obtained with pre-determined, generic rhythm-based rotational kinematics?
2) How do joint passive stiffness (bushing) property assumptions *[no bushing stiffness (NBS), generic linear bushing stiffness (LBS) or subject-specific, nonlinear bushing stiffness (NLBS)]* influence JRF estimates?
3) What is the effect of the assumed initial, zero pre-strain or "neutral" joint position (supine state vs. upright standing)?

2. Methods

2.1. Experimental data acquisition

The study utilizes a single volunteer's data from a previously published institutional review board (IRB)-approved study (Aiyangar et al., 2015; Aiyangar et al., 2014) . The volunteer (female; age 25; 60.8 kg; 176 cm) had performed a series of upright standing and straight-legged dynamic lifting tasks while holding 4.5 kg (10 lb) , 9.1 kg (20 lb) , and 13.6 kg (30 lb). During the tasks, the volunteer's lumbar spine (L2-S1) was simultaneously imaged in the sagittal and frontal planes by a DSX system (30 Hz, pulsed exposure = 4 ms/frame, excitation voltage = 70–80 kV, current = 320–630 mA, effective radiation dose per dynamic trial < 0.6 mS v) (Aiyangar et al., 2014) . Additionally, motion of the rest of the body was acquired by capturing displacements of 30 reflective markers placed on the participant's body with an 8-camera Vicon motion capture system, while two force plates (BERTEC, Columbus OH, USA) measured ground reaction forces.

Three-dimensional (3D) bone models of each lumbar vertebra were derived from high resolution computed tomography (CT) scans (voxel size = 0.25 mm × 0.25 mm × 1.25 mm, effective radiation dose < 12.3 mSv) of the participant's lumbar spine in supine position. Using a previously validated model-based tracking algorithm (precision <= 0.2 mm and 0.26°), the instantaneous 3D position and orientation of each vertebra were determined by registering the 3D bone model to the two 2D radiographs at each recorded frame (Lee, 2010). For further details, see (Aiyangar et al., 2015, 2017; 2014).

2.2. Subject-Specific musculoskeletal model development

A generic full-body musculoskeletal model was constructed in OpenSim by combining an existing lower- and upper-body model (Arnold et al., 2010; Senteler et al., 2015). Maximum muscle stress of each muscle was set to 100 N/cm^2 according to a recently published thoracolumbar spine model (Bruno et al., 2015). Virtual markers were added to the generic model to mimic those placed on the volunteer during data acquisition. The generic model was then scaled to the subject by maximizing correlation between virtual markers and experimental marker positions during upright standing using OpenSim's *Scale* tool as follows. First, body segments were scaled by size based on differences in location between experimental markers and the model's virtual markers. However, scaling by size did not ensure that the model mass matched the subject's measured mass. Hence, the model was scaled once more by mass to ensure that total model mass equaled measured mass.

Intervertebral lumbar motion was prescribed at each segment from L2L3 to L5S1. At each level, the joint's reference position and orientation with respect to each adjacent vertebra – termed the "neutral state" – was defined. The neutral state describes the intervertebral configuration where passive forces and torques are zero. Simulations were performed with two variations of the joint neutral state – upright- and supine-relative. For the "upright-relative" case, the DSX-measured upright standing, no external weight L2-S1 configuration was the neutral state. For the "supine-relative" case, the CT-measured supine L2-S1 configuration defined the neutral state. Segmental joint centers of rotation (COR) were defined to be approximately at the disc center, mainly to facilitate comparison of results to those derived from previous modeling studies using rhythm-based kinematic (Bruno et al., 2015; Bruno et al., 2017; Senteler et al., 2015) (Fig. 1).

As the raw DSX data describing lumbar intervertebral motion were in the form of body-fixed kinematics of the superior vertebral body coordinate system (CS) with respect to the inferior vertebral body CS, they were transformed to describe intervertebral motion with respect to the neutral state about the newly defined CORs. This transformation was performed for both the upright- and supine-relative neutral state models to ensure identical lumbar motion in space. By employing this methodology, the lumbar joints were essentially modeled as 6DOF joints allowing three orthogonal rotations about a moving COR capable of anterior-posterior (AP),

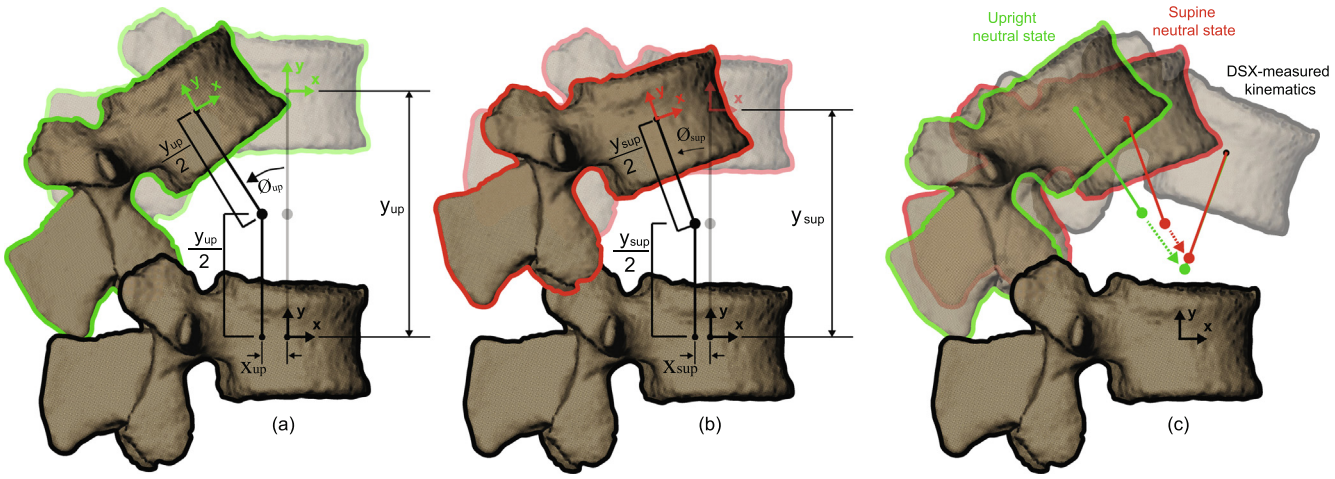

Fig. 1. Two variations of the joint "neutral state", where no forces or moments are present at the joint. The upright (a) and supine (b) neutral states represented the DSX-measured and CT-measured kinematics while the subject assumed the upright standing ($_{up}$) and supine ($_{sup}$) position, respectively. The neutral state kinematics were defined by a superior-inferior (SI) displacement (y_{up} or y_{sup}), anterior-posterior (AP) displacement (x_{up} or x_{sup}), and a flexion–extension (FE) angular displacement ($Ø_{up}$ or $Ø_{sup}$) between adjacent vertebrae. The joint centers from L2L3 to L4L5 were placed equidistant from- and orthogonally to each vertebra's local X- (AP) axis, in order to locate the joint center at the approximate geometric center of the disc. The relative orthogonal distances between the newly defined joint center and the local X-axes of L5 and S1 vertebrae were not equidistant, since the S1 coordinate system was placed at the superior surface of the sacrum, as opposed to the center of the vertebral body as done for the L2 to L5 vertebrae. Appropriate adjustments were accordingly made. y_{up} and y_{sup} represent the SI distance between vertebrae when no joint rotation is present. (c) The neutral state definition serves as the reference state in which the DSX kinematics are described.

superior-inferior (SI), and medial–lateral (ML) translations. Flexion-extension (FE), lateral bending (LB) and axial rotation (AR) (appropriately transformed as described above) were prescribed with respect to time based on the experimental dataset (Aiyangar et al., 2015; Aiyangar et al., 2014). In OpenSim®, COR translations are usually prescribed with respect to a generalized coordinate. Hence the AP, SI, and ML translations were implemented as coupled motions, and prescribed with respect to corresponding instantaneous FE rotation instead of time (See Appendix 1 for details).

Uncoupled stiffness matrices describing force- or moment-displacement relationships between consecutive bodies were defined at each joint from L2L3 to L5S1 for the linear (LBS) and nonlinear (NLBS) models (Table 1). For LBS models, rotational and translational stiffness constants were identical to those used in a previous musculoskeletal model (Senteler et al., 2015). NLBS model stiffness relationships were defined as spline functions based on force–displacement relationships derived from a displacement-controlled finite element (FE) study on the current subject's lumbar spine (Affolter, 2019) (Fig. 2)[1].

2.3. Kinematic and dynamic analyses

At each timeframe during the lifting motion, *Inverse Kinematics (IK)* was performed on the model to determine the joint angles necessary to achieve maximum correlation between the model's virtual marker set and the measured experimental surface marker positions. However, L2-S1 kinematics were explicitly prescribed based on DSX measurements and not allowed to be adjusted by the IK algorithm during this process. The sacrum was assumed to be rigidly attached to the pelvis. Since specific motion data for T12-L2 were not measured, motion from L12 and upwards was lumped with the thorax (C7-T12), which was assumed to be rigid (Arjmand, 2006; de Zee et al., 2007; Raabe and Chaudhari, 2016; Senteler et al., 2015). Pelvic motion (at the hip joint) itself was based on surface marker data, as were motions at the remaining joints such as shoulders, elbows, knees and ankles. This resulted in a motion file describing dynamic motion of all joints within the model during the entire lifting motion. *Inverse Dynamics (ID)* was then performed to determine the generalized forces and moments at each joint necessary to generate the IK-determined full-body motion according to:

$$M(q)\ddot{q} + C(q,\dot{q}) + G(q) = \tau$$

where: $q, \dot{q}, \ddot{q}$ = vectors of generalized positions, velocities, and accelerations, respectively; $M(q)$ = system mass matrix; $C(q,\dot{q})$ = Coriolis and centrifugal forces vector; $G(q)$ = vector of gravitational forces, including any external forces; τ = generalized forces vector (to be calculated).

A *Residual Reduction Algorithm (RRA)* was implemented to minimize modeling and surface marker processing errors and ensure consistency of model kinetics with measured ground reaction forces. In case of high residual forces, the torso center of mass and overall model mass were adjusted to keep residual forces at an acceptable level (<=30 N).

Subsequently, *Static Optimization (SO)* was performed to compute individual muscle at each time step. Muscle activation patterns were constrained to minimize the sum of muscle activation squared, which is approximately equivalent to minimizing total muscle stress. Lastly, *Joint Reactions Analysis (JRA)* was implemented to compute L4L5 JRF (See Appendix 3 for clarification on bushing force calculations). The same pipeline of analyses was implemented on 24 variations (Kinematics: 2 levels; Neutral state: 2 levels; Passive stiffness: 3 levels; Weight lifted: 2 levels; 2x2x3x2 = 24) of the subject-specific full-body model based on a single volunteer's dataset, wherein the following effects on L4L5 JRF and muscle forces were examined:

1) Lumbar kinematics: Generic, rhythmic (Rhy) vs. subject-specific 6-DOF DSX-measured kinematics (DSX). Rhythmic models consisted of no translational DOF. A constant ratio of lumbar segmental flexion–extension (FE) motion with respect to total L2–S1 FE motion was prescribed as done in a previously validated lumbar spine kinematic model (Senteler et al., 2018).

[1] This work presented at the 3rd International Workshop on Spine Loading and Deformation, Berlin, Germany July 2019 ("Estimating Lumbar Passive Stiffness Behavior from Subject-Specific Finite Element Models and In Vivo 6DOF Kinematics" Session 6: Spinal Loads, In Vivo Measurement and Modeling) and a manuscript has been submitted to the corresponding J. Biomechanics special issue.

Table 1
Uncoupled stiffness properties prescribed to each joint for both LBS and NLBS models.

Joint – Bushing type	AP (N/m)	SI (N/m)	ML (N/m)	LB (Nm/rad)	AR (Nm/rad)	FE (Nm/rad)
L23 – LBS	246,348	1783,989	135,000	64	268	37
L23 – NLBS	Fig. 2*a*	Fig. 2*b*	135,000	64	268	*from* Fig. 2*c*
L34 – LBS	148,855	1890,170	135,000	69	291	51
L34 – NLBS	Fig. 2*a*	Fig. 2*b*	135,000	69	291	*from* Fig. 2*c*
L45 – LBS	85,714	1962,000	135,000	94	293	65
L45 – NLBS	Fig. 2*a*	Fig. 2*b*	135,000	94	293	*from* Fig. 2*c*
L51 – LBS	386,511	1669,000	135,000	131	281	79
L51 – NLBS	Fig. 2*a*	Fig. 2*b*	135,000	131	281	*from* Fig. 2*c*

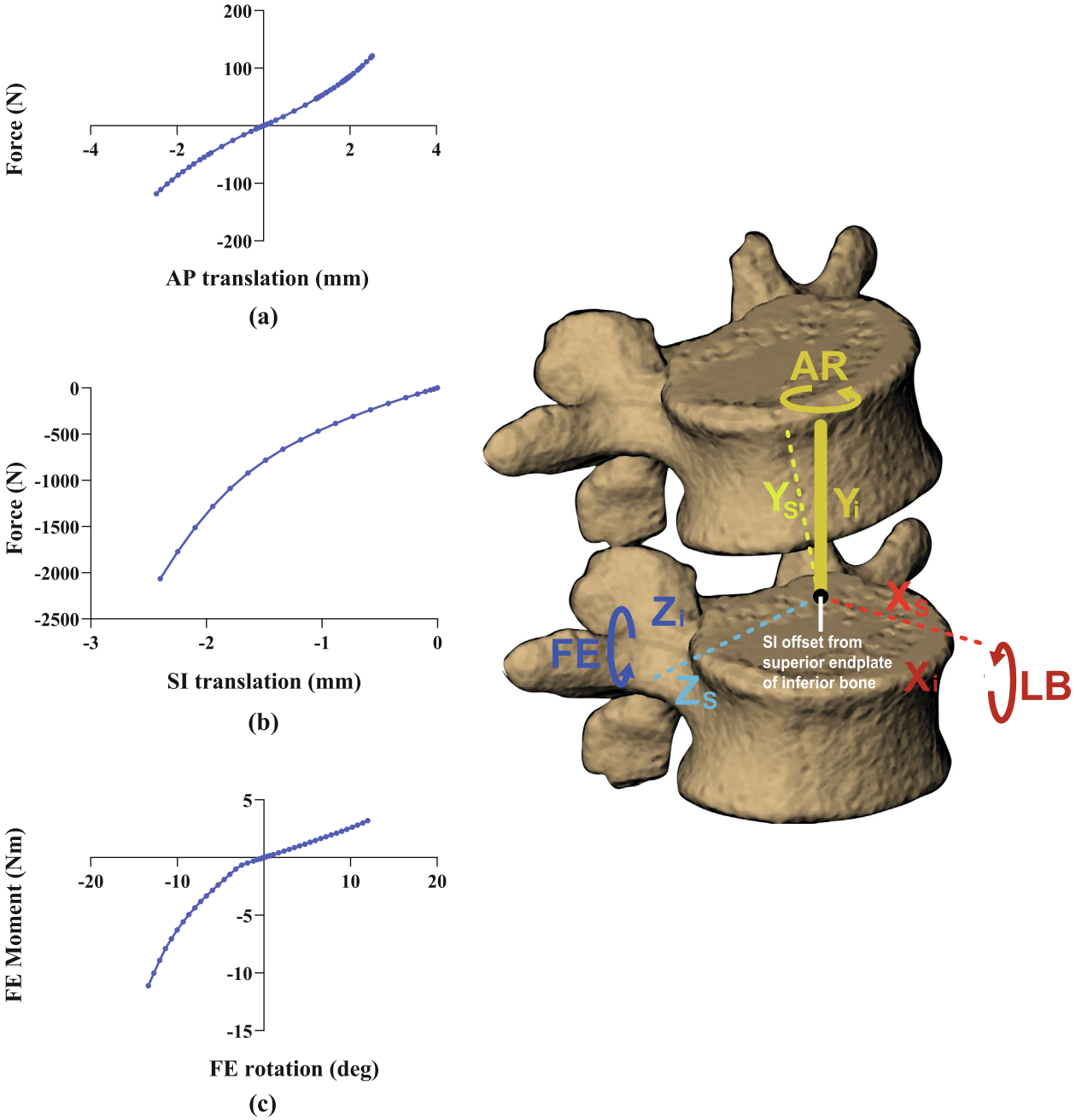

Fig. 2. Nonlinear stiffness curves for (a) anterior-posterior translation, (b) superior-inferior translation, and (c) flexion–extension rotation. Positive values along the x-axis correspond to anterior translation, superior translation, and extension of the superior vertebra with respect to the inferior vertebra for the AP translation, SI translation, and FE rotation motions, respectively. Positive forces and moments correspond to the anterior, superior, and extension directions, and are representative of the loads experienced by the inferior vertebra in the inferior vertebra coordinate system.

2) Neutral state: Supine (sup)-relative vs. upright (up) intervertebral joint "neutral state". This refers to whether the lumbar configuration at supine or upright standing position was used to define joint positions and orientations where no passive forces or moments are present (Fig. 1).
3) Intervertebral disc (bushing) stiffness: No bushing stiffness (NBS) vs. linear bushing stiffness (LBS) vs. nonlinear bushing stiffness (NLBS). LBS models utilized constant rotational and translational stiffness values at the lumbar joints according to those used in a previous study (Senteler et al., 2015). NLBS models prescribed intervertebral force–displacement relationships obtained from a concurrent displacement-controlled finite element study utilizing the same, subject-specific *in vivo* dataset (Affolter, 2019).
4) External load lifted: 10 lb (4.5 kg) vs. 30 lb (13.6 kg) load lifted during the lifting task.

3. Results

JRF from the 24 model variations based on a single subject's dataset are compiled to illustrate the sensitivity to choices made within the three primary input parameters: vertebral kinematics, passive stiffness and neutral state (Fig. 3). Differences due to interactions of choices made within the primary parameters are compiled in Tables 2–5. Additionally, absolute JRF for each model variation are made available in Supplemental Materials (Fig. A2) and (Tables A1, A2). Muscle forces estimates from the 24 model variations are also compiled in Supplemental Materials (Fig. A3, A4) and (Tables A3, A4), along with a description of results in Appendix 2.

4. Joint reaction forces

4.1. DSX vs Generic, rhythmic kinematics

JRF estimates were generally lower in DSX-based models compared to rhythm-based kinematics through most of the range of motion (ROM). Peak differences over the entire ROM reached 31% and 39% for compressive and shear JRF, respectively, when calculated based on assessing the *main effect* of this input type (Fig. 3a-b. Supplemental Figure A2a-d for absolute values). Secondly, assumptions with respect to passive stiffness properties

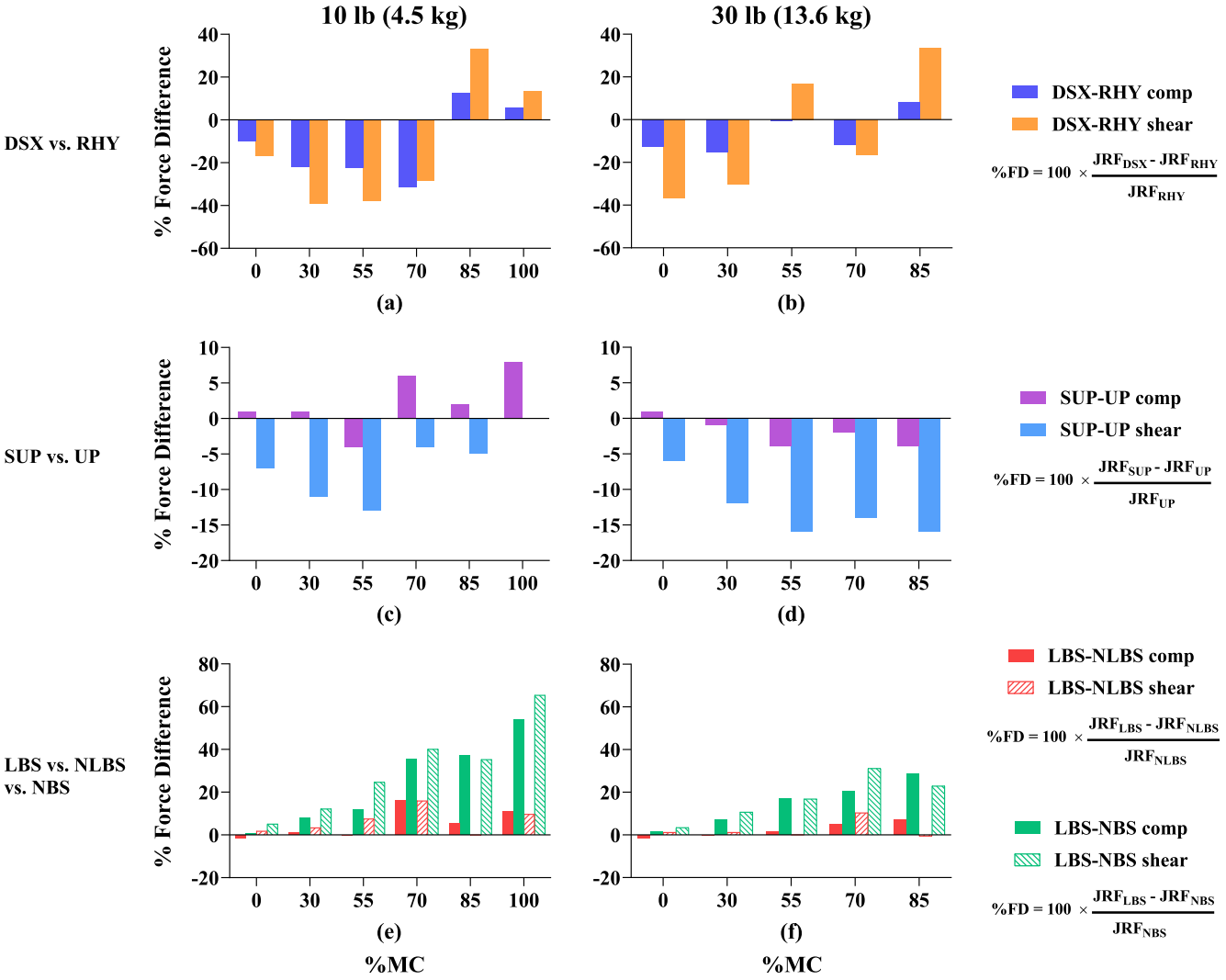

Fig. 3. Percent difference in compressive and shear L45 net JRF at several instances of percent motion completion (%MC) during the 10 lb and 30 lb lifts, where 0 %MC and 100%MC correspond to the flexed and upright posture of the subject, respectively. Results are presented with respect to the three main effects studied: DSX-based (DSX) vs. rhythm-based (RHY) input kinematics (top), supine joint neutral state (SUP) vs. upright joint neutral state (UP) (middle), and linear bushings (LBS) vs. nonlinear bushings (NLBS) vs. no bushings (NBS) (bottom).

Table 2
Percent differences in compressive and shear JRF due to different vertebral kinematic input in models of varying stiffness properties and joint neutral state. Percent difference was quantified as $100^{*}(JRF_{dsx} - JRF_{rhy})/JRF_{rhy}$. Values are shaded from largest decrease (red) to largest increase (blue), where no color indicates a 0% change.

		Supine						Upright					
		LBS		NLBS		NBS		LBS		NLBS		NBS	
	%MC	10	30	10	30	10	30	10	30	10	30	10	30
Compression	0	-10.2	-9.8	-11.9	-12.9	-9.4	-11.6	-8.7	-14.3	-11.7	-14.6	-7.9	-12.0
	30	-11.5	-6.9	-22.7	-13.5	-18.4	-12.6	-28.5	-20.8	-30.5	-21.0	-17.9	-14.4
	55	-21.9	12.9	-24.4	5.4	-8.3	0.4	-30.7	-6.0	-31.6	-9.0	-12.1	-6.8
	70	6.6	1.0	-37.6	-13.0	-31.2	-4.7	-41.3	-16.8	-49.6	-22.8	-32.7	-11.0
	85	31.9	20.0	15.7	0.5	3.4	2.7	10.7	10.9	7.1	4.7	2.1	9.0
	100	30.4		0.7		-5.4		3.8		-1.1		-2.1	
Shear	0	-19.2	-26.6	-17.5	-33.5	-13.4	-40.8	-12.0	-42.1	-20.1	-40.4	-18.4	-37.4
	30	-27.9	-15.0	-36.2	-21.4	-34.1	-29.9	-43.4	-37.5	-48.4	-38.1	-42.7	-34.8
	55	-5.9	41.6	-33.3	43.0	-24.2	29.3	-52.0	3.3	-55.0	-0.2	-42.0	2.6
	70	25.3	13.6	-29.3	-9.5	-11.4	-15.0	-48.2	-19.2	-52.2	-34.4	-35.4	-26.0
	85	48.0	26.5	45.0	31.5	46.9	28.9	17.8	35.1	23.1	35.5	27.4	44.2
	100	20.6		4.0		8.6		24.0		7.3		13.3	

Table 3
Percent differences in compressive and shear JRF due to bushing stiffness properties in *supine neutral state models* of varying kinematic input. Percent difference was quantified as $100^{*}(JRF_{factor1} - JRF_{factor2})/JRF_{factor2}$, where "factor1" vs. "factor2" is the comparison being made. Values are shaded from largest decrease (red) to largest increase (blue), where no color indicates a 0% change.

		DSX						RHY					
		LBS vs NBS		NLBS vs NBS		NLBS vs LBS		LBS vs NBS		NLBS vs NBS		NLBS vs LBS	
	%MC	10	30	10	30	10	30	10	30	10	30	10	30
Compression	0	-0.1	4.0	0.8	2.8	0.9	-1.2	0.8	2.0	3.7	4.4	2.8	2.3
	30	15.6	13.8	3.6	7.7	-10.4	-5.3	6.6	6.8	9.4	8.9	2.6	2.0
	55	0.1	31.1	-1.8	23.8	-1.8	-5.6	17.4	16.6	19.1	17.9	1.4	1.1
	70	92.4	29.8	13.1	12.2	-41.2	-13.6	24.2	22.5	24.9	22.9	0.5	0.3
	85	81.3	53.0	58.0	27.5	-12.8	-16.7	42.2	30.9	41.3	30.2	-0.6	-0.5
	100	122.4		68.2		-24.4		61.3		58.0		-2.1	
Shear	0	-3.0	27.9	-1.1	16.1	2.0	-9.2	3.9	3.2	3.9	3.4	0.0	0.2
	30	19.1	33.5	6.0	24.1	-11.0	-7.1	8.9	10.2	9.6	10.8	0.6	0.5
	55	48.5	32.3	6.3	34.6	-28.4	1.8	19.7	20.8	20.8	21.8	0.9	0.8
	70	83.6	71.6	4.0	37.1	-43.4	-20.1	29.9	28.5	30.3	28.8	0.3	0.2
	85	58.7	38.1	54.8	42.9	-2.4	3.5	57.5	40.7	56.9	40.0	-0.4	-0.4
	100	104.3		73.7		-15.0		83.9		81.3		-1.4	

and the neutral state modulated these differences (Table 2. Absolute values in Supplemental Materials Tables A1 & A2) with differences reaching almost 50% in some instances.

4.2. Passive stiffness properties

LBS- and NLBS model-based compressive and shear JRF estimates were consistently larger than NBS model predictions, with differences increasing substantially towards the end of the lifting task, respectively (Fig. 3e-f. See Supplemental Figure A2i-l for absolute values). Overall, differences between LBS and NLBS models were smaller compared to corresponding differences with NBS models outputs, particularly in the rhythm-based kinematic models (Tables 3, 4). Secondly, differences between the LBS and NLBS model JRF estimates were smaller in the rhythm-based kinematic models compared to the DSX-based models.

4.3. Supine vs upright neutral state

The *main effect* of *neutral state* was the smallest of the three primary input factors (Fig. 3c-d): peak difference in shear JRF estimates was 16% or less. However, there were strong interactions with the choice of kinematic input and bushing type. Peak differences in shear JRF increased to 30% with rhythm-based kinematic input and were even larger in DSX-based models with LBS bushings (Table 5).

4.4. Intervertebral input kinematics

Differences in intervertebral kinematics at the upright and supine positions – as captured by DSX and CT, respectively – led to slight differences in upright- and supine-relative input kinematics. Flexion-extension (FE) kinematics at the L4L5 were shifted approximately two degrees (more negative) when described with respect to the upright position compared to the supine position (Fig. 4).

5. Discussion

The current study elaborated the steps implemented for incorporating 6DOF subject-specific kinematics and passive stiffness properties into a full-body OpenSim® musculoskeletal model. While no specific validation studies were conducted, estimated

Table 4
Percent differences in compressive and shear JRF due to bushing stiffness properties in *upright neutral state models* of varying kinematic input. Percent difference was quantified as $100^{*}(JRF_{factor1} - JRF_{factor2})/JRF_{factor2}$, where "factor1" vs. "factor2" is the comparison being made. Values are shaded from largest decrease (red) to largest increase (blue), where no color indicates a 0% change.

		DSX						RHY					
		LBS vs NBS		NLBS vs NBS		NLBS vs LBS		LBS vs NBS		NLBS vs NBS		NLBS vs LBS	
	%MC	10	30	10	30	10	30	10	30	10	30	10	30
Compression	0	0.7	-0.1	0.0	1.7	-0.7	1.8	1.6	2.5	4.3	4.8	2.7	2.2
	30	-0.7	3.7	-1.4	5.3	-0.7	1.5	13.9	12.0	16.5	14.1	2.3	1.8
	55	-0.6	24.4	-0.8	21.6	-0.2	-2.3	26.0	23.4	27.5	24.5	1.2	0.9
	70	16.0	17.6	-0.2	9.3	-14.0	-7.1	32.9	25.8	33.2	26.0	0.2	0.2
	85	58.6	34.4	52.1	26.0	-4.1	-6.2	46.4	32.0	45.0	31.1	-0.9	-0.7
	100	73.1		61.2		-6.9		63.2		59.5		-2.3	
Shear	0	13.5	-3.8	3.3	-0.7	-9.0	3.3	5.2	4.0	5.4	4.3	0.2	0.3
	30	13.1	9.4	3.9	9.2	-8.1	-0.2	14.5	14.1	15.5	15.0	0.8	0.8
	55	7.2	27.5	1.3	24.0	-5.5	-2.7	29.5	26.5	30.6	27.5	0.9	0.7
	70	12.0	42.4	3.5	15.7	-7.6	-18.8	39.6	30.4	39.8	30.5	0.2	0.1
	85	50.0	30.3	55.8	30.0	3.9	-0.2	62.3	39.1	61.2	38.3	-0.7	-0.6
	100	109.4		78.4		-14.8		91.2		88.4		-1.5	

Table 5
Percent differences in compressive and shear JRF due to joint neutral state in models of varying kinematic input and stiffness properties. Percent difference was quantified as $100^{*}(JRF_{sup} - JRF_{up})/JRF_{up}$. Values are shaded from largest decrease (red) to largest increase (blue), where no color indicates a 0% change.

		DSX						RHY					
		LBS		NLBS		NBS		LBS		NLBS		NBS	
	%MC	10	30	10	30	10	30	10	30	10	30	10	30
Compression	0	-0.7	4.2	0.8	1.1	0.1	0.1	1.0	-1.0	1.1	-0.8	1.8	-0.4
	30	16.3	9.6	5.0	2.2	-0.1	-0.1	-5.9	-6.8	-5.7	6.6	0.5	-2.2
	55	0.9	5.2	-0.8	1.7	0.2	-0.1	-10.5	-12.4	-10.3	12.3	-3.9	-7.3
	70	67.1	10.4	14.2	2.7	0.7	0.1	-7.9	-9.1	-7.7	9.0	-1.5	-6.6
	85	14.3	5.0	3.9	-6.7	0.0	-7.8	-4.1	-2.9	-3.8	2.8	-1.2	-2.1
	100	29.5		5.2		0.8		3.1		3.3		4.3	
Shear	0	-14.5	16.8	-4.1	2.7	0.1	-12.2	-6.9	-7.8	-7.1	-8.0	-5.7	-7.1
	30	4.3	9.1	1.0	1.6	-0.9	-10.6	-18.1	-19.8	-18.3	-20.0	-13.9	-16.9
	55	38.8	-5.3	5.2	-0.9	0.2	-8.7	-29.2	-30.9	-29.1	-30.8	-23.3	-27.6
	70	79.4	3.3	9.9	1.6	9.4	-14.3	-25.8	-26.5	-25.7	-26.4	-20.2	-25.4
	85	6.7	-17.4	0.2	-14.4	0.9	-22.1	-15.1	-11.9	-14.9	-11.7	-12.5	-12.8
	100	-1.0		-1.2		1.4		1.8		1.9		5.8	

L4L5 JRF magnitudes were within bounds reported by previous studies examining lumbar flexion or lifting tasks (Arshad et al., 2017; Beaucage-Gauvreau et al., 2019; Eskandari et al., 2017; Kingma et al., 2016). Maximum compressive and shear loads ranged from approximately 2400 N – 3300 N and 475 N – 1000 N, respectively, across all model variations.

Although comparatively more modest, previous modeling studies investigating effects of ignoring translations have reported similar trends as in the current study. For example, (Ghezelbash et al., 2015) reported a low-to-moderate effect of ignoring translational DOF on JRF predictions (~15% for compression and ~36% for shear) in a custom-developed nonlinear finite element-based model of the lumbar spine (Arjmand and Shirazi-Adl, 2005, 2006). Deploying a force-dependent-kinematics (FDK) approach with an OpenSim®-based upper trunk model (Bruno et al., 2015; Meng et al., 2015) showed a modest reduction in compressive force estimates with coupled stiffness models for the intervertebral bushings; the estimates were much more sensitive to rotational stiffness values than translational stiffnesses. (Arshad et al., 2017) demonstrated modest (7%) reductions in compressive force estimates at L4L5 when translational stiffnesses (and, implicitly, translational DOF) were incorporated into an AnyBody®-based model (de Zee et al., 2007) with an FDK approach. (Bruno et al., 2017) demonstrated the sensitivity of predicted forces to assumed spinal curvature. Incorporating CT-derived subject-specific spinal curvatures resulted in a median difference of approximately 15% in computed compressive forces at the L3 level compared to a generic, scaled model based on subject's height and weight, when simulating a 40° flexed posture with a 10 kg weight. This parameter is analogous to the neutral state parameter in our study. Somewhat similar to the current study, (Eskandari et al., 2017) drove their spine model with single plane fluoroscopy-based kinematics, with CT-based supine posture as the initial, unloaded state and compared results to a generic, rhythm-based kinematics-driven model. However, that study only reported modest differences (<15%) in compression force estimates over several static postures, although relatively larger differences

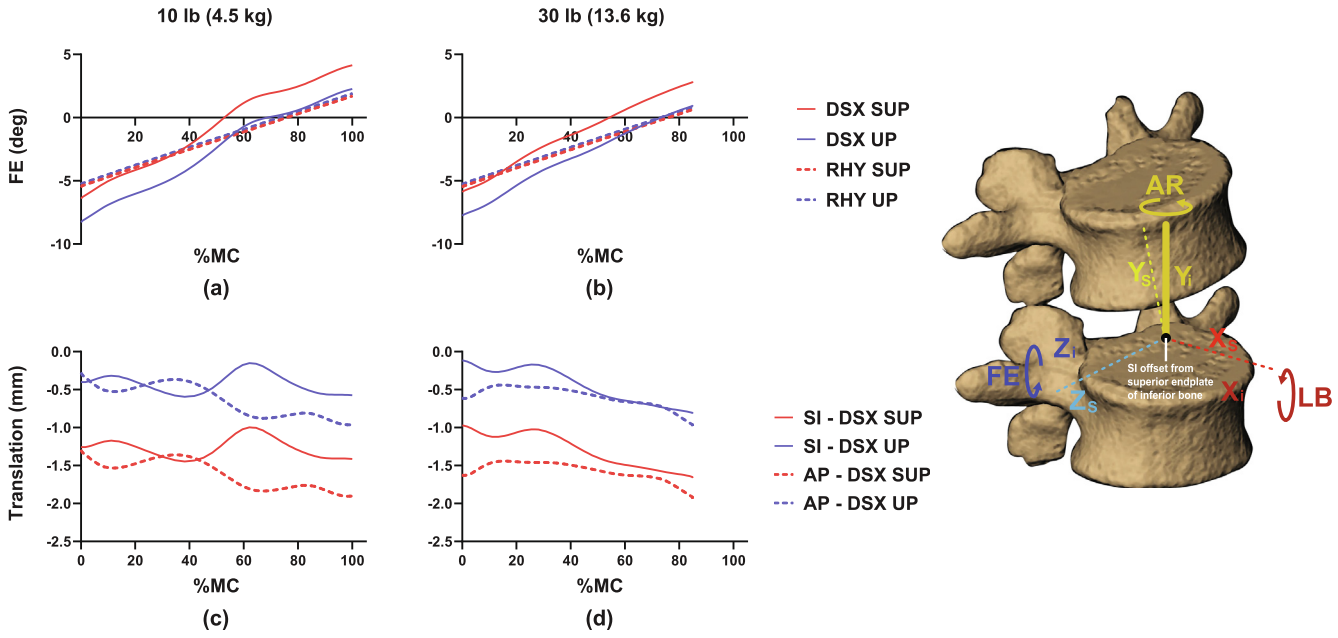

Fig. 4. (a) and (c) display the L4L5 flexion–extension (FE) rotational and translational motions for the 10 lb trial, while (b) and (d) display the FE rotational and translational motions for the 30 lb trial, respectively. Positive values correspond to extension, superior, and anterior directions. FE rotations varied with respect to the joint's neutral state and kinematic input, while SI and AP translations were zero for rhythmic models.

in local lumbar muscle forces were found. The aforementioned works were all based on inverse static models, with most limited to investigating specific, single poses.

Building on these past studies, the current study demonstrates how, compared to generic inputs, subject-specific kinematics, intervertebral disc stiffness, and joint neutral state definition can alter model estimates of net joint reaction loads and muscle forces in the lumbar spine during a functional, dynamic task.

Interestingly, compressive force estimates from the current, inverse dynamics-based study were not substantially different from those of the above-mentioned inverse static analyses. However, estimated shear forces (up to ~1000 N) were several times larger than (Eskandari et al., 2017), (Arshad et al., 2017) and (Bruno et al., 2017), who reported shear forces in the range of 50 N – 150 N. (Dehghan-Hamani et al., 2019) reported a slightly wider range of L4L5 shear forces (42 N – 342 N) in five subjects at a trunk (T12) flexion angle of ~46° using inverse static analysis; however corresponding compressive force estimates (~890 N – 1390 N) were comparatively lower. The current study's shear JRF are closer in magnitude and range to recent inverse dynamics-based analyses of lifting tasks (~650 N – 1600 N) (Beaucage-Gauvreau et al., 2019; Kingma et al., 2016). Inverse dynamics analyses account for additional contributions to the net joint moments from acceleration and inertial effects, which are ignored in inverse static analyses. This appears to exert a much stronger influence on shear force estimates than on compressive forces.

In general, implementing 6DOF DSX-based kinematics predicted lower JRF compared to a generic, rhythm-based distribution of lumbar segmental motion without translational DOF through approximately two-thirds of the ROM, with equal or slightly higher JRF in the final third. This result is consistent with a previous musculoskeletal modeling study, which showed that the optimal COR location for minimizing JRF may vary for each instantaneous flexed position of the lumbar spine (Senteler et al., 2018). A preceding analysis of instantaneous CORs using the finite helical axis method also showed that these CORs migrated over the range of the lifting motion (Aiyangar et al., 2017). Since rhythm-based models had no translations, the fixed joint CORs could have additionally constrained the model, resulting in larger JRF estimates.

The effects of bushing stiffness on lumbar loads were highly dependent on the model's kinematic input. Surprisingly, inclusion of bushing stiffnesses (LBS or NLBS) led to larger net JRF estimates than those calculated from NBS models, particularly in the final third of the ROM. There are two possible explanations for these seemingly counter-intuitive results. First, the L4L5 segment was in a flexed orientation in the first half of the motion, transitioning to an extended orientation in the final third (Fig. 4). This is significant for models implementing rotational stiffnesses, as the reaction moment of an extended joint will act in the flexion direction, placing an additional moment, which the muscles must account for to achieve the desired kinematics. Second, non-sagittal components of the 6DOF motion seemed to generate larger muscle forces consequently resulting in increased joint reaction forces overall. We tested this notion by creating an additional LBS model (LBS_{SAG}) with sagittal-only kinematics and stiffnesses – extension rotation, anterior-posterior and superior-inferior translations. Differences in JRF between LBS_{SAG} and NBS models occurred exactly as expected: compared to LBS_{SAG}, JRF in NBS models were larger during the first half of the lift (flexed segmental orientation), and smaller during the final third (extended segmental orientation). However, including lateral bending, axial rotation, and medial–lateral translation DOF and stiffnesses (LBS model) resulted in an additional increase in JRF at the joint throughout the lifting motion (Fig. 5). Thus, even small non-sagittal rotational and translational motions seemed to require greater muscle forces to stabilize the non-sagittal external moments. The combined effect of these two factors resulted in a small increase in the LBS/NLBS model-based JRF estimates compared to NBS in the first half of the motion, which was exacerbated in the final third. Additionally, this behavior may also have contributed to confounding the general observation of lower forces in the DSX-based models compared to the rhythm-based ones in the final third of the ROM.

Overall, although model outputs were least sensitive to the neutral position, effects were magnified with specific combinations of

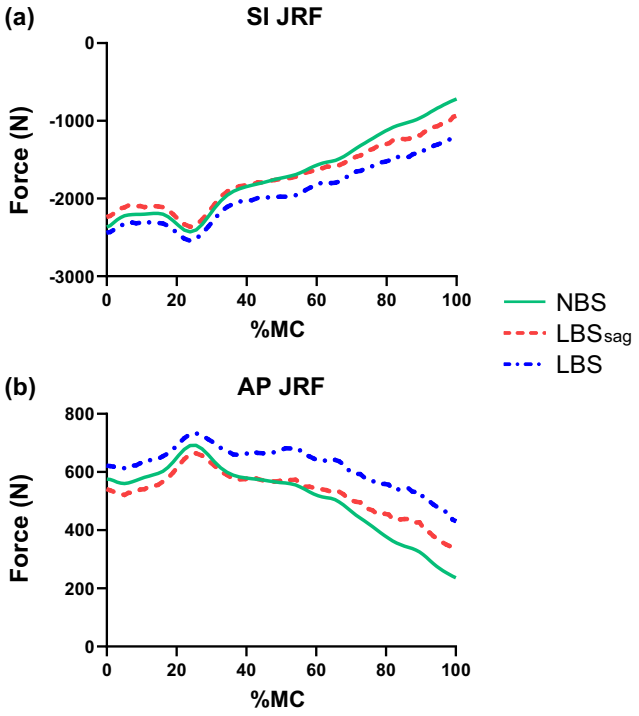

Fig. 5. Superior-inferior joint reaction forces in 3 models throughout the lifting motion, with respect to percent motion completion (%MC). Anterior-posterior joint reaction forces in 3 models throughout the lifting motion, with respect to percent motion completion (%MC). NBS = No Bushing Stiffness; LBS_{sag} = Linear Bushing Stiffness (only sagittal plan stiffness and DOF); LBS = Linear Bushing Stiffness.

passive stiffness and kinematic input (whether subject-specific or generic). These results demonstrate the need for further characterization of the pre-stressed state of the intervertebral joint.

While much effort was put into incorporating accurate *in vivo* data, there remain a few limitations within the musculoskeletal models used in this study. First, the current study focuses on a single subject's data. While the results from this study cannot be considered representative of a population, they were useful in laying out the study's methodology and demonstrating the effects of - and interactions between - the studied parameters. Second, intra-abdominal pressure, which has been shown to affect load estimates in the lumbar spine, was not included in this study. However, this is a parameter which will be included in future studies on a larger sample size to better represent *in vivo* conditions. Further, ligaments were not explicitly modeled; instead, the passive stiffness properties included in the model were meant to represent the entire passive joint structure. Lastly, as the focus of the current study was on the portion of the lumbar spine measured by DSX, individual segmental motions T12-L1 and between the sacrum and pelvis were neglected.

The study not only highlights model sensitivity to choices made regarding the three primary input parameters—kinematics, passive stiffness and neutral state— separately, but also how the interactions between each of these choices can result in significant variability in joint loading estimates over the entire range of a given dynamic task. The results provide some evidence that inclusion of translational joint motion could lead to reduced compressive and shear JRF during flexion/extension of the lumbar spine. However, a more "accurate" dataset for one of the inputs (e.g. segmental kinematics) might also heighten the demand for accuracy of the accompanying input variables such as passive stiffness properties and presumed joint neutral position.

Acknowledgements

This work was supported by a research grant (R21OH00996) from the Centers for Disease Control and Prevention/National Institute for Occupational Safety and Health (CDC/NIOSH) and an *Ambizione* Career Grant Award (PZ00P2_154855/1) from the Swiss National Science Foundation (SNSF).

OpenSim® is funded by NIH Roadmap grant U54 GM072970, the NIH research infrastructure grant R24 HD065690, and the DARPA Warrior Web Program.

Conflict of Interest Statement

The authors have no conflict of interest (e.g. consultancies, stock ownership, equity interests, patent-licensing arrangements) related to the manuscript or the work it describes.

Appendix 1. – Transformation of intervertebral kinematics

Body-fixed DSX transformation of superior vertebra with respect to inferior vertebra:

$$\begin{bmatrix} x' \\ y' \\ z' \end{bmatrix} = R_z R_y R_x \begin{bmatrix} x \\ y \\ z \end{bmatrix} + \begin{bmatrix} T_x \\ T_y \\ T_z \end{bmatrix}$$

However, the location of the vertebral origin is $\begin{bmatrix} 0 \\ 0 \\ 0 \end{bmatrix}$, so the position of the superior vertebra origin after transformation is simply

$$\begin{bmatrix} x' \\ y' \\ z' \end{bmatrix} = \begin{bmatrix} T_x \\ T_y \\ T_z \end{bmatrix}$$

The raw DSX-derived data described intervertebral motion by ordered body-fixed rotations of the superior vertebral body coordinate system with respect to the inferior vertebral body coordinate system. However, in our OpenSim model we have modeled the lumbar joints such that the superior vertebral body rotates about a joint center between adjacent vertebrae, as opposed to its own vertebral coordinate system during Euler body-fixed rotations. Furthermore, we have added an anterior-posterior (AP) translation and flexion–extension (FE) rotation between adjacent vertebrae. Due to the change in joint representation, prescribing the same exact values of rotations and translations to the joint would result in different spatial locations and orientations of the superior vertebra with respect to the inferior vertebra. Therefore, we must account for this when prescribing joint motion so that we can orient and position the vertebrae identically in space to that measured by DSX.

Accounting for the difference in angular orientation is rather straightforward. Regardless of whether a body is rotating about its own coordinate system axes or those of another coordinate system, if the coordinate systems are angularly oriented identically the resulting angular orientation after rotational transformation of the body will remain the same; only the position of the body in space will differ. For our modeled joints, the only angular orientation adjusted when defining the neutral state of the joint is the FE rotation. Since FE rotation is the first ordered body-centered rotation in the DSX-derived data, applying the appropriate amount of FE rotation from the neutral state about the joint center – in this case, the DSX-derived FE rotation plus the *opposite* FE rotation present at the neutral state – will orient the superior vertebral coordinate axes exactly as the DSX-derived body-fixed FE rotation would

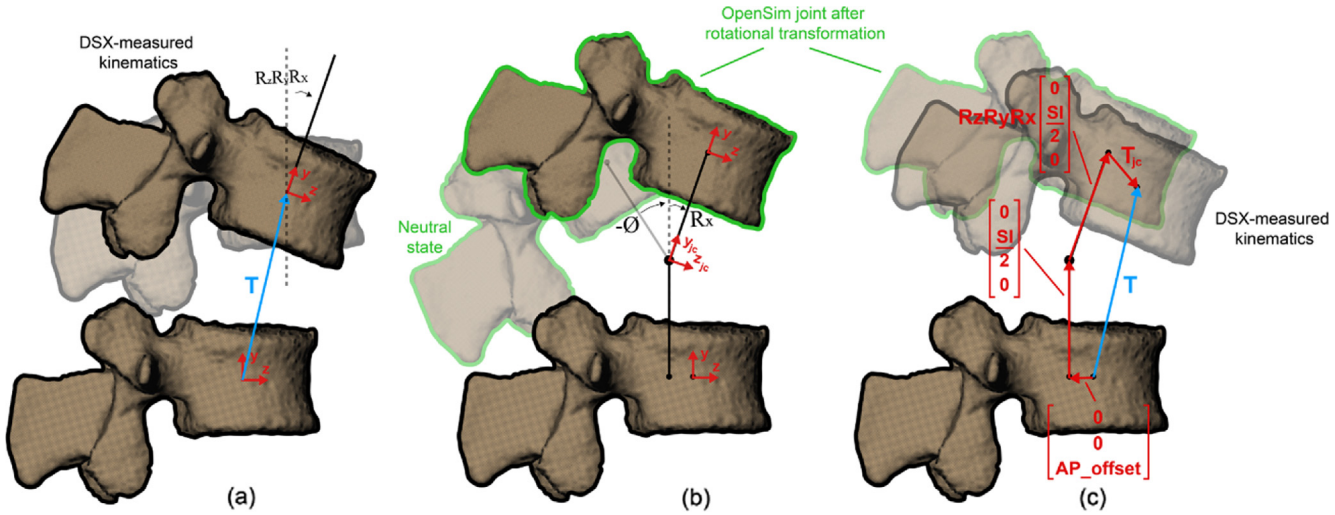

Fig. A1. Due to a different representation of intervertebral kinematics between DSX and our OpenSim model joints, an additional FE rotation and translational vector was added when prescribing joint kinematics. (a) DSX kinematics were described by ordered body-fixed rotations, with flexion–extension (FE) being the first of the three angle rotations, followed by a body-fixed transformation vector. (b) In our model of the lumbar joint, the neutral state definition introduces an angular offset between adjacent vertebra of the magnitude (ϕ). An FE rotation of $-\phi + Rx$ is applied to align the coordinate axes of the superior vertebra as they would be oriented after a body-fixed FE rotation via the DSX data. Thereafter, the AR and LB rotations are prescribed to the OpenSim joint. (c) After accounting for the joint's position in the neutral state, and the displacement of the superior vertebra in space due to the prescribed rotations, one can solve for the prescribed translation (Tjc) necessary to place the superior vertebra in the exact location as measured by DSX.

(Fig. A1). Thereafter, the values of AR and LB as measured by DSX can be directly prescribed about the joint center to match the angular orientation of the superior vertebra in space measured by DSX. However, as previously stated, since the OpenSim joint is rotating about a joint center and not its own anatomical axes, the superior vertebra will not be *positioned* correctly.

To place the superior vertebra of the L2L3 to L4L5 joints in the same respective position in space in OpenSim, but with respect to the joint center, an additional translational vector must be applied (*jc*):

$$\begin{bmatrix} x' \\ y' \\ z' \end{bmatrix} = \begin{bmatrix} T_x \\ T_y \\ T_z \end{bmatrix} = R_z R_y R_x \begin{bmatrix} 0 \\ SI/2 \\ 0 \end{bmatrix} + \begin{bmatrix} 0 \\ SI/2 \\ 0 \end{bmatrix} + \begin{bmatrix} 0 \\ 0 \\ AP\_offset \end{bmatrix} + \begin{bmatrix} T_{jc\_x} \\ T_{jc\_y} \\ T_{jc\_z} \end{bmatrix}$$

Solving the expression for the joint center translational vector leads to:

$$\begin{bmatrix} T_{jc\_x} \\ T_{jc\_y} \\ T_{jc\_z} \end{bmatrix} = \begin{bmatrix} T_x \\ T_y \\ T_z \end{bmatrix} - R_z R_y R_x \begin{bmatrix} 0 \\ SI/2 \\ 0 \end{bmatrix} - \begin{bmatrix} 0 \\ SI/2 \\ 0 \end{bmatrix} - \begin{bmatrix} 0 \\ 0 \\ AP\_offset \end{bmatrix}$$

For the L5S1 joint, the process is identical except that the distance between the joint center and the inferior and superior vertebral centres is SI/5 and 4*SI/5, respectively.

$$\begin{bmatrix} T_{jc} \\ T_{jc} \\ T_{jc} \end{bmatrix} = \begin{bmatrix} T_x \\ T_y \\ T_z \end{bmatrix} - R_z R_y R_x \begin{bmatrix} 0 \\ 4 * SI/5 \\ 0 \end{bmatrix} - \begin{bmatrix} 0 \\ SI/5 \\ 0 \end{bmatrix} - \begin{bmatrix} 0 \\ 0 \\ AP\_offset \end{bmatrix}$$

Appendix 2. – Muscle forces

Peak MF, LT, IL, and abdominal muscle forces reached 840 N, 1400 N, 1100 N, and 630 N, respectively, during the lifting tasks. While variation in the grouping of muscle fascicles complicates comparison across studies, muscle forces appeared to be within range of those calculated by previous studies (Arshad et al., 2017; Eskandari et al., 2017).

DSX vs rhythmic kinematics

Predicted muscle forces in models with DSX input kinematics showed uniquely different trends compared to models with a rhythmic kinematics distribution (Fig. A3, A4). The most striking differences were observed in the abdominal muscles, as the inclusion of DSX kinematics led to much larger muscle forces at specific instances of L2-S1 extension in the 10 lb and 30 lb lifts. This observation was consistent across all bushing stiffness types and held true regardless of the neutral state of the model (Tables A3, A4). In general, multifidus (MF) and Longissimus Thoracis (LT) forces substantially increased due to the inclusion of DSX kinematics, while Iliocostalis Lumborum (IL) forces decreased (Fig. a3c-d; Tables A3, A4).

Passive stiffness properties

Effects of passive stiffness properties varied across muscle groups. While only subtle differences in MF, LT, and IL forces were observed in models with rhythmic kinematics, a substantial increase in abdominal forces occurred with the inclusion of LBS or NLBS bushings. However, differences between LBS and NLBS models were negligible. In models with DSX kinematic input, differences due to passive stiffness varied throughout the lifting motion. For example, LBS models with the supine neutral state displayed larger IL forces compared to NLBS and NBS models at 70% MC during the 10 lb lift; however such differences were mitigated with the upright neutral state (Tables A3, A4). In general, it was difficult to pinpoint consistent trends due to variation of bushing stiffness properties in DSX models. Closer to the upright position, models with bushing forces included tended to predict higher MF and ABD forces compared to NBS models (Fig. A4e-f; Tables A3, A4).

Supine vs upright neutral state

Neutral state had a minimal effect on MF and LT muscle forces. However, differences in ABD and IL forces due to neutral state were considerable, particularly during the latter half of the lifting

motion. Similar to the effects on JRF, the sensitivity of model outputs to neutral state depended strongly on the type of kinematic input. Relative to DSX models, changes in muscle forces due to neutral state were minimally affected in rhythmic models (Tables A3, A4).

Appendix 3. Bushing – Force calculations

This section presents a brief clarification on bushing (IVD) force calculations and their incorporation into net JRF calculations in the *Joint Reaction Analysis* (JRA) step in OpenSim®. Joint *Reactions Analysis* in OpenSim, is a *post hoc* calculation, which determines the resultant forces and moments carried by all *un-modeled* joint structures required to produce the specified joint kinematics. Thus, the decision to either include or exclude certain structural components of the joint within the model will directly affect the resultant loads calculated by JRA. In a purely rigid body dynamics analysis of the lumbar joint – where no passive soft tissue structures are modeled (NBS model) – these forces, referred to as *net joint reaction forces*, collectively represent the *total* load to be resisted by all passive structures within that joint. In this study, we have also explicitly modeled passive disc (and ligament) stiffness by prescribing either linear (LBS) or nonlinear (NLBS) bushing-based force-kinematic relationships at the joint. Under this scenario, the *modeled bushing structure* generated resisting forces are already subtracted to provide *net* JRF output. Hence this value will not represent the *total* load acting at that particular joint. In order to obtain the *total* JRF in LBS and NLBS models and allow comparison with the corresponding the NBS model output, we must add the *modeled* passive (bushing) forces back to the *net* JRF output.

Appendix A. Supplementary material

Supplementary data to this article can be found online at https://doi.org/10.1016/j.jbiomech.2020.109659.

References

Affolter, C.A., Kedzierska, J., Vielma, T., Weisse, B.H., Ameet Aiyangar, A.K., 2019. Estimating Lumbar Passive Stiffness Behaviour from Subject-Specific Finite Element Models and In Vivo 6DOF Kinematics. 3rd International Workshop on Spine Loading and Deformation, Berlin, DE.

Aiyangar, A., Zheng, L., Anderst, W., Zhang, X., 2015. Apportionment of lumbar L2–S1 rotation across individual motion segments during a dynamic lifting task. J. Biomech. 48, 3709–3715.

Aiyangar, A., Zheng, L., Anderst, W., Zhang, X., 2017. Instantaneous centers of rotation for lumbar segmental extension in vivo. J. Biomech. 52, 113–121.

Aiyangar, A., Zheng, L., Tashman, S., Anderst, W., Zhang, X., 2014. Capturing three-dimensional in vivo lumbar intervertebral joint kinematics using dynamic stereo-X-ray imaging. J. Biomech. Eng. 136.

Arjmand, N., 2006. Model and in vivo studies on human trunk load partitioning and stability in isometric forward flexions. J. Biomech. 39, 510–521.

Arjmand, N., Shirazi-Adl, A., 2005. Biomechanics of changes in lumbar posture in static lifting. Spine (Phila Pa 1976) 30, 2637–2648.

Arjmand, N., Shirazi-Adl, A., 2006. Model and in vivo studies on human trunk load partitioning and stability in isometric forward flexions. J Biomech 39, 510–521.

Arnold, E.M., Ward, S.R., Lieber, R.L., Delp, S.L., 2010. A model of the lower limb for analysis of human movement. Ann Biomed Eng 38, 269–279.

Arshad, R., Zander, T., Bashkuev, M., Schmidt, H., 2017. Influence of spinal disc translational stiffness on the lumbar spinal loads, ligament forces and trunk muscle forces during upper body inclination. Med. Eng. Phys. 46, 54–62.

Bazrgari, B., Shirazi-adl, A., Trottier, M., Mathieu, P., 2008. Computation of trunk equilibrium and stability in free flexion â€“ extension movements at different velocities. Vivo 41, 412–421.

Beaucage-Gauvreau, E., Robertson, W.S.P., Brandon, S.C.E., Fraser, R., Freeman, B.J.C., Graham, R.B., Thewlis, D., Jones, C.F., 2019. Validation of an OpenSim full-body model with detailed lumbar spine for estimating lower lumbar spine loads during symmetric and asymmetric lifting tasks. Comput Methods Biomech Biomed Engin 22, 451–464.

Breen, A., Breen, A., 2018. Uneven intervertebral motion sharing is related to disc degeneration and is greater in patients with chronic, non-specific low back pain: an in vivo, cross-sectional cohort comparison of intervertebral dynamics using quantitative fluoroscopy. Eur Spine J 27, 145–153.

Bruno, A.G., Bouxsein, M.L., Anderson, D.E., 2015. Development and Validation of a Musculoskeletal Model of the Fully Articulated Thoracolumbar Spine and Rib Cage. J Biomech Eng 137, 081003.

Bruno, A.G., Mokhtarzadeh, H., Allaire, B.T., Velie, K.R., De Paolis Kaluza, M.C., Anderson, D.E., Bouxsein, M.L., 2017. Incorporation of ct-based measurements of trunk anatomy into subject-specific musculoskeletal models of the spine influences vertebral loading predictions. J Orthop Res.

Christophy, M., Faruk Senan, N.A., Lotz, J.C., O'Reilly, O.M., 2012. A musculoskeletal model for the lumbar spine. Biomech Model Mechanobiol 11, 19–34.

de Zee, M., Hansen, L., Wong, C., Rasmussen, J., Simonsen, E.B., 2007. A generic detailed rigid-body lumbar spine model. J. Biomech. 40, 1219–1227.

Dehghan-Hamani, I., Arjmand, N., Shirazi-Adl, A., 2019. Subject-specific loads on the lumbar spine in detailed finite element models scaled geometrically and kinematic-driven by radiography images. Int. J. Numer. Methods Biomed. Eng. 35.

Delp, S.L., Anderson, F.C., Arnold, A.S., Loan, P., Habib, A., John, C.T., Guendelman, E., Thelen, D.G., 2007. OpenSim: open-source software to create and analyze dynamic simulations of movement. IEEE Trans Biomed Eng 54, 1940–1950.

Eskandari, A.H., Arjmand, N., Shirazi-Adl, A., Farahmand, F., 2017. Subject-specific 2D/3D image registration and kinematics-driven musculoskeletal model of the spine. J. Biomech. 57, 18–26.

Eskandari, A.H., Arjmand, N., Shirazi-Adl, A., Farahmand, F., 2019. Hypersensitivity of trunk biomechanical model predictions to errors in image-based kinematics when using fully displacement-control techniques. J Biomech.

Gardner-Morse, M.G., Stokes, I.A.F., 2004. Structural behavior of human lumbar spinal motion segments. J. Biomech. 37, 205–212.

Ghezelbash, F., Arjmand, N., Shirazi-Adl, A., 2015. Effect of intervertebral translational flexibilities on estimations of trunk muscle forces, kinematics, loads, and stability. Comput Methods Biomech Biomed Engin 18, 1760–1767.

Ghezelbash, F., Eskandari, A.H., Shirazi-Adl, A., Arjmand, N., El-Ouaaid, Z., Plamondon, A., 2018. Effects of motion segment simulation and joint positioning on spinal loads in trunk musculoskeletal models. J Biomech 70, 149–156.

Han, K.S., Kim, K., Park, W.M., Lim, D.S., Kim, Y.H., 2013. Effect of centers of rotation on spinal loads and muscle forces in total disk replacement of lumbar spine. Proc. Inst. Mech. Eng. [H] 227, 543–550.

Kingma, I., Faber, G.S., van Dieen, J.H., 2016. Supporting the upper body with the hand on the thigh reduces back loading during lifting. J Biomech 49, 881–889.

Lee, J.B., E.; Anderst, W.J., 2010. Lumbar Spine Motion During Functional Movement. In: Vivo Validation of Flexion/Extension Movement Tracking, 3rd Annual Lumbar Spine ResearchSociety Meeting, Chicago, IL, USA.

Meng, X., Bruno, A.G., Cheng, B., Wang, W., Bouxsein, M.L., Anderson, D.E., 2015. Incorporating Six Degree-of-Freedom Intervertebral Joint Stiffness in a Lumbar Spine Musculoskeletal Model-Method and Performance in Flexed Postures. J Biomech Eng 137, 101008.

Panjabi, M.M., Oxland, T.R., Yamamoto, I., Crisco, J.J., 1994. Mechanical behavior of the human lumbar and lumbosacral spine as shown by three-dimensional load-displacement curves. J. Bone Joint Surg. 76, 413–424.

Pearcy, M.J., Bogduk, N., 1988. Instantaneous axes of rotation of the lumbar intervertebral joints. Spine 13, 1033–1041.

Raabe, M.E., Chaudhari, A.M.W., 2016. An investigation of jogging biomechanics using the full-body lumbar spine model: Model development and validation. J. Biomech. 49, 1238–1243.

Senteler, M., Aiyangar, A., Weisse, B., Farshad, M., Snedeker, J.G., 2018. Sensitivity of intervertebral joint forces to center of rotation location and trends along its migration path. J Biomech 70, 140–148.

Senteler, M., Weisse, B., Rothenfluh, D.A., Snedeker, J.G., 2015. Intervertebral reaction force prediction using an enhanced assembly of OpenSim models. Comput. Methods Biomech. Biomed. Eng., 1–11

Seth, A., Hicks, J.L., Uchida, T.K., Habib, A., Dembia, C.L., Dunne, J.J., Ong, C.F., DeMers, M.S., Rajagopal, A., Millard, M., Hamner, S.R., Arnold, E.M., Yong, J.R., Lakshmikanth, S.K., Sherman, M.A., Ku, J.P., Delp, S.L., 2018. OpenSim: Simulating musculoskeletal dynamics and neuromuscular control to study human and animal movement. PLoS Comput Biol 14, e1006223.

Seth, A., Sherman, M., Reinbolt, J.A., Delp, S.L., 2011. OpenSim: a musculoskeletal modeling and simulation framework for in silico investigations and exchange. Procedia IUTAM 2, 212–232.

Sherman, M.A., Seth, A., Delp, S.L., 2013. What Is a Moment Arm? Calculating Muscle Effectiveness in Biomechanical Models Using Generalized Coordinates. Proc ASME Des Eng Tech Conf 2013.

Tafazzol, A., Arjmand, N., Shirazi-Adl, A., Parnianpour, M., 2014. Lumbopelvic rhythm during forward and backward sagittal trunk rotations: combined in vivo measurement with inertial tracking device and biomechanical modeling. Clin Biomech (Bristol, Avon) 29, 7–13.

Xia, Q., Wang, S.B., Kozanek, M., Passias, P., Wood, K., Li, G.A., 2010. In-vivo motion characteristics of lumbar vertebrae in sagittal and transverse planes. J. Biomech. 43, 1905–1909.

Zanjani-Pour, S., Meakin, J.R., Breen, A., Breen, A., 2017. Estimation of in vivo inter-vertebral loading during motion using fluoroscopic and magnetic resonance image informed finite element models. J Biomech.